Original Article

The value of predicting the invasiveness and degree of infiltration of pulmonary ground-glass nodules based on computed tomography features and enhanced quantitative analysis

Bingkun Xie[#], Rong Wang[#], Kunyue Fu, Qian Wang, Zhenhe Liu, Wenting Peng

Department of Radiology, Qilu Hospital of Shandong University Dezhou Hospital, Dezhou, China

Contributions: (I) Conception and design: B Xie, R Wang; (II) Administrative support: B Xie, R Wang, Q Wang; (III) Provision of study materials or patients: B Xie, R Wang, W Peng; (IV) Collection and assembly of data: K Fu, Q Wang, Z Liu; (V) Data analysis and interpretation: K Fu, Q Wang, W Peng; (VI) Manuscript writing: All authors; (VII) Final approval of manuscript: All authors.

[#]These authors contributed equally to this work.

Correspondence to: Qian Wang, MS. Department of Radiology, Qilu Hospital of Shandong University Dezhou Hospital, No. 1166 of Dongfanghong Road, Decheng District, Dezhou 253000, China. Email: wang_qian111@yeah.net.

Background: The incidence and mortality rate of lung cancer are the highest in the world among all malignant tumors. Accurate assessment of ground-glass nodules (GGNs) is crucial in reducing lung cancer mortality. This study aimed to explore the value of computed tomography (CT) features and quantitative parameters in predicting the invasiveness and degree of infiltration of GGNs.

Methods: Lesions were classified into three groups based on pathological types: the precursor glandular lesion (PGL) group, including atypical adenomatoid hyperplasia and adenocarcinoma *in situ*; the minimally invasive adenocarcinoma group; and the invasive adenocarcinoma group. Quantitative and qualitative data of the nodules were compared, and receiver operating characteristic (ROC) curve analysis was performed for each quantitative parameter. Binary logistic regression analysis was used to evaluate independent predictors of GGN invasiveness.

Results: There were significant differences in lesion size, morphology, nodule type, bronchial abnormality, internal vascular sign and pleural retraction among the three groups ($P<0.05$). There were significant differences in all CT quantitative parameters (CT attenuation value in the plain phase, CT attenuation value in the arterial phase, CT attenuation value in the venous phase, arterial phase enhancement difference, venous phase enhancement difference, arterial phase enhancement index and venous phase enhancement index) among the three groups ($P<0.001$). The ROC curve analysis showed that the CT attenuation value in the plain phase, CT attenuation value in each enhanced phase, enhancement difference and enhancement index had good discriminatory power. Binary logistic regression analysis revealed that nodule type and internal vascular sign were independent risk factors for GGN invasiveness.

Conclusions: CT features combined with enhanced scanning and quantitative analysis have important value in predicting the invasiveness of GGNs. The type of pulmonary nodule detected on CT (pure GGN or mixed GGN) and the presence of internal vascular signs are independent risk factors for GGN invasiveness.

Keywords: Pulmonary ground-glass nodules (pulmonary GGNs); tomography; X-ray computed; computed tomography feature (CT feature)

Submitted Nov 30, 2023. Accepted for publication Jul 11, 2024. Published online Aug 23, 2024.
doi: 10.21037/qims-23-1708
View this article at: https://dx.doi.org/10.21037/qims-23-1708

Introduction

Lung cancer has the highest incidence and mortality rate in the world, with adenocarcinoma being the most common, accounting for about 50–60% of lung cancers (1,2). According to statistics, lung cancer has become the most common type of cancer in China, accounting for almost 30% of cancer-related deaths (3,4). Therefore, early screening for lung cancer has become an important disease prevention task. With the widespread use of computed tomography (CT) in lung cancer screening, more and more ground-glass nodules (GGNs) have been detected in the lung, which is the most common presentation of early lung adenocarcinoma (5-8). According to the 2021 World Health Organization (WHO) Classification of Lung Tumors (5th edition), lung epithelial tumors are classified according to pathological histology into precursor glandular lesions (PGLs) [including atypical adenomatoid hyperplasia (AAH) and adenocarcinoma in situ (AIS)], minimally invasive adenocarcinoma (MIA) and invasive adenocarcinoma (IAC) (9). For the different types of GGN, there are significant differences in prognosis and therefore different treatment strategies. For example, the clinical treatment for PGL is close follow-up or local wedge resection, and after complete resection, the 10-year survival rate reaches 100%; conversely, MIA can transform into IAC, and the clinical treatment is usually segmental resection or lobectomy, and the patient's postoperative 5-year survival rate is close to 100%; however, once stage I lung cancer enters into IAC, the clinical treatment is lobectomy plus lymph node dissection, and its 5-year survival rate can be reduced to 73–90% (10,11). The importance of early screening for lung cancer is self-evident. CT is an important tool for early screening of lung cancer, and early and accurate identification of the invasiveness and degree of infiltration of lung nodules on CT images is crucial in determining the patient's follow-up, timing of intervention and prognosis. A CT plain scan is commonly used in the diagnosis of pulmonary nodules, but it has some limitations in the diagnosis of benign and malignant pulmonary nodules (12). The study shows that the enhanced CT scan can differentiate the nature of the nodules more accurately and further improve diagnostic sensitivity and accuracy. Furthermore, an enhanced spiral CT scan can provide more reliable evidence of the relationship between the blood supply of pulmonary nodules and the peripheral blood vessels, thus providing more reliable evidence for clinical treatment (13). Scholars (14) have pointed out that the combination of plain CT with the qualitative and quantitative parameters of enhanced scans has important predictive value in predicting the malignancy and invasiveness of pulmonary GGNs. Therefore, this study aims to investigate the value of CT features and enhanced quantitative analysis in predicting the invasion and degree of infiltration of GGNs and to provide a reference for the clinical development of appropriate treatment modalities. We present this article in accordance with the STROBE reporting checklist (15) (available at https://qims.amegroups.com/article/view/10.21037/qims-23-1708/rc).

Methods

Clinical data

Patients who underwent pulmonary nodule resection in our hospital between January 2019 and June 2023 were retrospectively analysed, and all pathological specimens were obtained by thoracoscopic or open thoracic surgery. The inclusion criteria were as follows: (I) CT manifestation of GGNs, and the maximum diameter of the nodule was ≤3 cm; (II) the patient underwent pulmonary nodule resection, and the presence of pulmonary nodules was confirmed by postoperative pathology; (III) the patient underwent a CT plain scan and enhanced scan within 2 weeks before surgery. The exclusion criteria were as follows: (I) the patient underwent a puncture biopsy or anti-tumor treatment, such as radiotherapy or chemotherapy, before the CT examination; (II) the images were of poor quality, which affected the diagnostic effect. The study was conducted in accordance with the Declaration of Helsinki (as revised in 2013). The study was approved by the Ethics Committee of Qilu Hospital of Shandong University Dezhou Hospital (Ethics Approval No. 2023009), and individual consent for this retrospective analysis was waived.

Examination methods

The GE Optima 64-row CT scanner (GE Company, Norwalk, CT, USA) was used, the supine position was routinely taken and all patients were scanned after holding their breath at the end of inspiration. Scanning parameters (16): automatic exposure dose-adjusted scanning mode, tube voltage 80–120 kV, automatic milliampere second and a conventional layer thickness of 5 mm were used for scanning. All lung window images were reconstructed using a sharp algorithm, and mediastinal window images were reconstructed using a standard algorithm for thin-

layer reconstruction with a reconstruction layer spacing of 1.25 mm and a reconstruction slice thickness of 1.25 mm. The lung window was set to [1,500, −550 Hounsfield unit (HU)] and the mediastinum was set to (350, 40 HU) for viewing. Enhancement scanning was performed using a non-ionic iodine contrast agent with an automatic tracking-triggered scanning technique at an injection rate of 3.0 mL/s and a dose of 1.0–1.5 mL/kg, the descending aortic threshold was monitored after the injection, the arterial phase was scanned with a delay of 12 s after manual or automatic triggering and the venous phase was scanned at 25 s.

Image analysis

All images were transferred to the PACS workstation, and the CT images were analysed by two senior attending chest diagnostic radiologists with no prior knowledge of the patient's pathological diagnosis; in case of disagreement, a consensus was reached after discussion with another more experienced senior radiologist. Using lung window observation, some CT signs were subjected to multi-directional observation by technical means, such as multiplanar reformation. Radial measurement and volume identification of GGNs were assisted by the intelligent diagnostic module of lung nodules in the AI-assisted diagnostic system (uAI software of Shanghai Lianzhi Company, version: 430sp2).

Qualitative parameters included the following (17,18)
(I) Type of nodule [0 for pure GGN (pGGN), 1 for mixed GGN (mGGN)]. Type pGGN refers to the slightly high-density fuzzy shadow of ground-glass opacity on the lung window, which does not cover the display of blood vessels and bronchi, does not contain any solid components and the mediastinal window is invisible. Type mGGN refers to the light GGNs with solid components, which can be nodules and spots with patchy density increase shadows, covering adjacent blood vessels and some solid lesions can be displayed in the mediastinal window); (II) morphology (0 for round nodule, 1 for irregular nodule); (III) tumor-lung interface (0 for clear and smooth nodule, 1 for rough and blurred nodule); (IV) bronchial abnormality (0 for no nodule in the bronchiolar pathway, 1 for bronchial abnormalities, such as bronchospasm, narrowness and dilatation, and the CT scan shows increased and thickened lung markings); (V) vacuole sign (0 for nodule with no vacuole sign, 1 for nodule with vacuole sign); (VI) internal vascular sign (0 for no vascular entry, detour or normal vascular routing within the nodule, 1 for vascular anomaly, where vascular entry into the lesion is twisted, stiff or has thickened routing); (VII) pleural retraction (0 for no records, 1 for records).

Quantitative parameters included the following
(I) GGN short diameter, long diameter, mean diameter and volume; (II) CT attenuation value in the plain scan, CT attenuation value in the arterial phase of enhancement, CT attenuation value in the venous phase of enhancement [measurements were made on CT plain scan and enhancement scanning transverse-axis lung window thin-layer images, selecting the largest level, the region of interest (ROI), trying to include an area of two-thirds of the nodule and avoiding the blood vessels and bronchial tubes]; (III) the degree of enhancement (CT attenuation value arterial phase – CT attenuation value plain scan, noted as ΔCT A-N; CT attenuation value venous phase – CT attenuation value plain scan, noted as ΔCT V-N); (IV) intensification index (intensification index A: CT arterial/CT surrounding normal lung tissue arterial; intensification index V: CT venous/CT surrounding normal lung tissue venous). All the measurements were performed by the same two senior attending chest diagnostic radiologists mentioned above. In case of disagreement, a consensus was reached after discussion with the same senior radiologist mentioned above.

Pathological examination

Specimens were completed in the Department of Pathology, Shandong University Qilu Hospital, Dezhou Hospital, and the final pathological diagnosis was determined by two pathologists with the seniority of attending physician or above. According to the new WHO lung adenocarcinoma classification standard of 2021 (9), the 136 GGNs were divided into the PGL (AAH + AIS) group, MIA group and IAC group. The infiltrative subtypes of lung adenocarcinoma included AAH, which was mild-to-moderate atypical hyperplasia of the epithelial cells in the lesion without interstitial inflammatory reaction and fibroplasia; AIS, which showed wall-mounted growth of tumor cells along the alveoli without interstitial, vascular or pleural infiltration; MIA, which had a predominantly wall-mounted growth pattern, showing isolated and infiltrative extent ≤0.5 cm; IAC was adenocarcinoma of the lung in which there was invasion of the interstitium, blood vessels

and pleura with an infiltrating range of >0.5 cm.

Statistical analysis

The data were processed and analysed using SPSS 26.0 statistical software, and the normality of the measurements was analysed using the Kolmogorov-Smirnov test. Measurements that conformed to the normal distribution were expressed as ($\bar{x}$±s), and one-way analysis of variance and independent samples *t*-test were used; those that were not normally distributed were expressed as M (Q1, Q3), and non-parametric tests were used (H test). Count data were analysed using the Chi-squared test, and multiple comparisons between groups, and P<0.05 was considered a statistically significant difference. Receiver operating characteristic (ROC) curve analysis was performed for quantitative data, the area under the curve (AUC) was calculated and thresholds and their corresponding sensitivity and specificity were determined based on the maximum Yoden index. Binary logistic regression analysis was used to assess the independent predictors of GGN invasiveness and degree of infiltration.

Results

General data and CT imaging features of the three groups of patients with GGNs

In this study, based on the inclusion and exclusion criteria, 126 patients with CT manifestation of GGNs were finally selected, with a total of 136 nodules. These comprised 32 men and 94 women aged 30–81 years, with a mean age of (57.8±11.0) years. Fifty-one cases were type pGGN, 85 were type mGGN, 40 patients were in the PGL group, 41 were in the MIA group and 55 were in the IAC group (*Figure 1A-1D*). Gender, lesion location distribution, smoking history, vacuole sign and tumor-lung interface did not show statistically significant differences among the three groups (P=0.776, 0.637, 0.406, 0.104, 0.431, respectively); lesion size, morphology, nodule type, bronchial abnormality, internal vascular sign, pleural retraction and other characteristic indexes showed statistically significant differences among the three groups (P<0.05) (*Table 1*). The infiltrating lesion (MIA and IAC) radii and volumes were significantly higher than those of PGL, and the comparisons between groups were statistically significant (P<0.05); the results of the ROC curves showed that the nodal radii and volumes had a high predictive efficacy of invasion of GGNs and a slightly lower predictive efficacy of the degree of infiltration (*Figure 2A,2B*, *Table 2*). The proportion of mGGNs and signs of vascular abnormality tended to increase with the increase in the degree of infiltration, and all comparisons between groups were statistically significant (P<0.05). The proportions of the presence of irregular morphology and signs of bronchial abnormality in the IAC group were significantly higher than those in the MIA group and the PGL group (P<0.05), and the proportions of the presence of signs of pleural tugging in the IAC group were significantly higher than those in the PGL group in both cases (P<0.05).

Comparison of quantitative indices of scanning and enhanced CT among the three groups

The overall differences in quantitative CT indices (scanning CT attenuation value, arterial-phase CT attenuation value, venous-phase CT attenuation value, arterial-phase enhancement difference ΔCT A-N, venous-phase enhancement difference ΔCT V-N, intensification index A and intensification index V) were statistically significant between the three groups as well as in a two-by-two comparison between the three groups (P<0.001) (*Table 3*).

ROCs curve analysis

The statistically significant quantitative indexes were subjected to ROC curve analysis, and the results showed that the CT attenuation value of plain scan, the CT attenuation value of each stage of enhancement, the enhancement difference and the intensification index all had high predictive efficacy for the invasion of GGNs (*Figure 3A*) and slightly lower predictive efficacy for the degree of infiltration (*Figure 3B*, *Table 4*); the enhancement of the venous stage of the CT attenuation value for distinguishing between the PGL and invasive lesions had the highest prediction efficacy. The enhanced venous CT attenuation values had the highest predictive efficacy, with an optimal threshold value of −452.16 HU, an AUC of 0.841, a sensitivity of 68.8% and a specificity of 90.0%; in addition, the predictive efficacy of the enhancement difference and the intensification index V was slightly higher than that of the enhanced CT attenuation values (*Tables 2,4*).

Binary logistic regression analysis

The parameters of lung nodule size, nodule type,

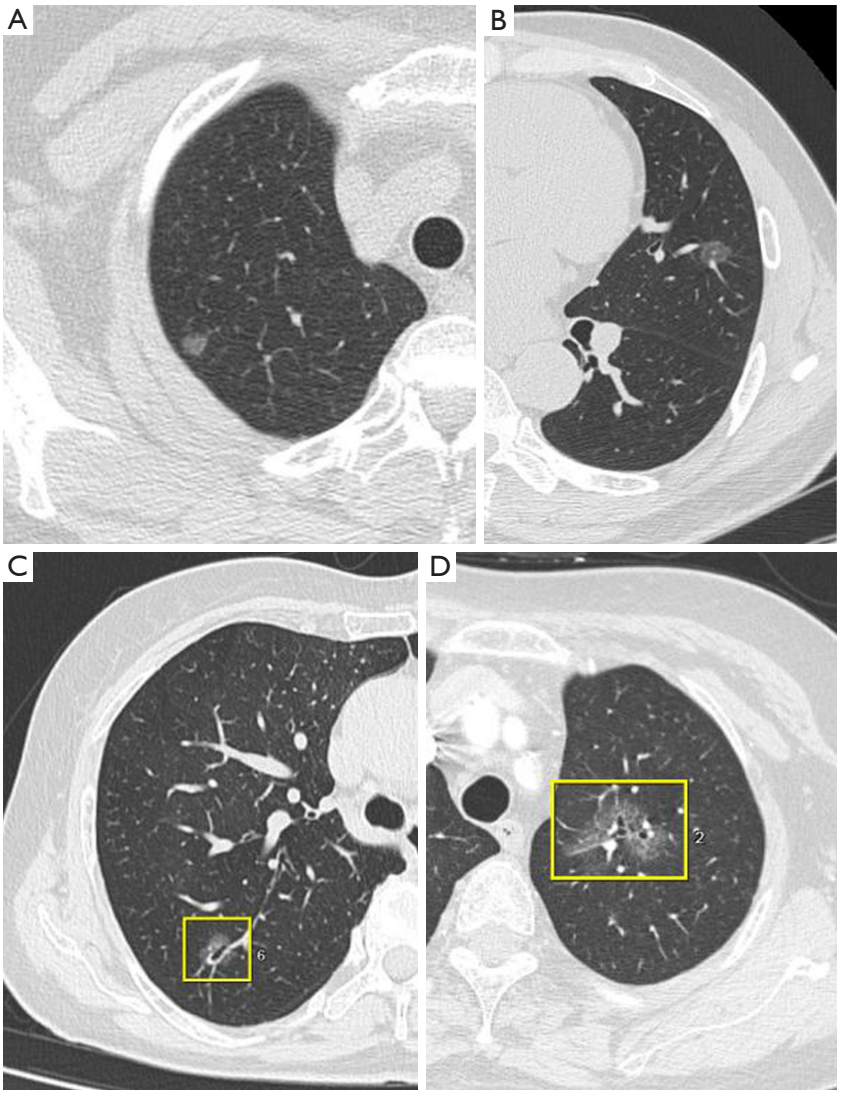

Figure 1 CT imaging features. (A) Female, 57 years old, AAH, round GGN in the apical segment of the right upper lobe of the lung, with a maximum cross-section of approximately 0.6 cm × 0.7 cm and clear borders. (B) Male, 46 years old, AIS, frosted glass nodule in the inferior lingual segment of the upper lobe of the right lung, measuring approximately 1.3 cm × 1.1 cm, with the lesion partially encircling a blood vessel. (C) Female, 69 years old, MIA, a partial solid nodule in the posterior segment of the upper lobe of the right lung, approximately 1.3 cm × 1.2 cm in size, with a visible inflated bronchial sign. Yellow box: a partial solid nodule. (D) Female, 71 years old, IAC. a partial solid nodule in the upper lobe of the right lung, approximately 3.0 cm × 2.1 cm in size, with visible air bronchogram. Yellow box: a partial solid nodule. CT, computed tomography; AAH, atypical adenomatoid hyperplasia; GGN, ground-glass nodules; AIS, adenocarcinoma in situ; MIA, minimally invasive adenocarcinoma; IAC, invasive adenocarcinoma.

morphology, bronchial abnormality sign, internal vascular sign and pleural retraction were included in the binary logistic regression analysis with non-infiltrative (AAH + AIS) and infiltrative (MIA + IAC) as the dependent variables, and the results showed that the nodule type [odds ratio (OR) =14.026, 95% confidence interval (CI) 4.916–40.020, P<0.001] and internal vascular sign (OR =6.346, 95% CI: 1.860–21.646, P=0.003) were independent risk factors for GGN invasion. Using MIA and IAC as dependent variables, the parameters of lung nodule size, nodule type, morphology, bronchial abnormality sign, internal vascular sign and pleural retraction were included

Table 1 General data and CT imaging features of the three groups of GGN patients

Groups	Precursor glandular lesion (n=40)	Minimally invasive adenocarcinoma (n=41)	Invasive adenocarcinoma (n=55)	Statistical value	P
Sex				0.507	0.776
Male	9_a	12_a	15_a		
Female	31_a	29_a	40_a		
Age (years), mean ± SD [range]	54.03±10.53 [30–75]	58.56±11.81 [32–81]	61.48±8.78 [37–78]	6.037	0.003
Lesion location distribution				0.901	0.637
Right lung	27_a	28_a	33_a		
Left lung	13_a	13_a	22_a		
Smoking history				1.803	0.406
Currently smokes or formerly smoked	4_a	6_a	11_a		
Never smoked	36_a	35_a	44_a		
Lesion size (mm)					
Short caliber	7.40 (2.78)	10.00 (3.50)	15.30 (7.00)	54.245	<0.001
Longitudinal	9.30 (4.10)	12.90 (5.80)	19.70 (11.50)	61.220	<0.001
Average diameter	8.30 (3.24)	11.55 (4.63)	17.65 (10.50)	60.740	<0.001
Volume (mm^3)	329.87 (392.77)	800.29 (1,053.05)	3,066.84 (3,465.47)	50.085	<0.001
Nodule type, n (%)				54.965	<0.001
pGGN	32_a (80.0)	16_b (39.0)	3_c (5.5)		
mGGN	8_a (20.0)	25_b (61.0)	52_c (94.5)		
Morphology, n (%)				51.358	<0.001
Round or oval	34_a (85.0)	27_a (65.9)	8_b (14.5)		
Irregular	6_a (15.0)	14_a (34.1)	47_b (85.5)		
Tumor-lung interface				1.684	0.431
Clear and smooth	37_a	35_a	46_a		
Rough and fuzzy	3_a	6_a	9_a		
Bronchial abnormality, n (%)				49.147	<0.001
Yes	3_a (7.5)	6_a (14.6)	38_b (69.1)		
No	37_a (92.5)	35_a (85.4)	17_b (30.9)		
Vacuole sign, n (%)				4.531	0.104
Yes	7_a	8_a	19_a		
No	33_a	33_a	36_a		
Internal vascular sign, n (%)				41.576	0.006
Yes	4_a (10.0)	17_b (41.5)	42_c (76.4)		
No	36_a (90.0)	24_b (58.5)	13_c (23.6)		
Pleural retraction, n (%)				7.264	0.026
Yes	13_a (32.5)	18_{ab} (43.9)	33_b (60.0)		
No	27_a (67.5)	23_{ab} (56.1)	22_b (40.0)		

Data was presented as mean ± standard deviation or number. Non-parametric tests are expressed as median (interquartile range); each subscripted letter represents the result after multiple comparisons between groups; where the same letter is labeled, there is no statistically significant difference in the comparison between groups (P>0.05). CT, computed tomography; GGN, ground-glass nodules; pGGN, pure ground-glass nodules; mGGN, mixed ground-glass nodules.

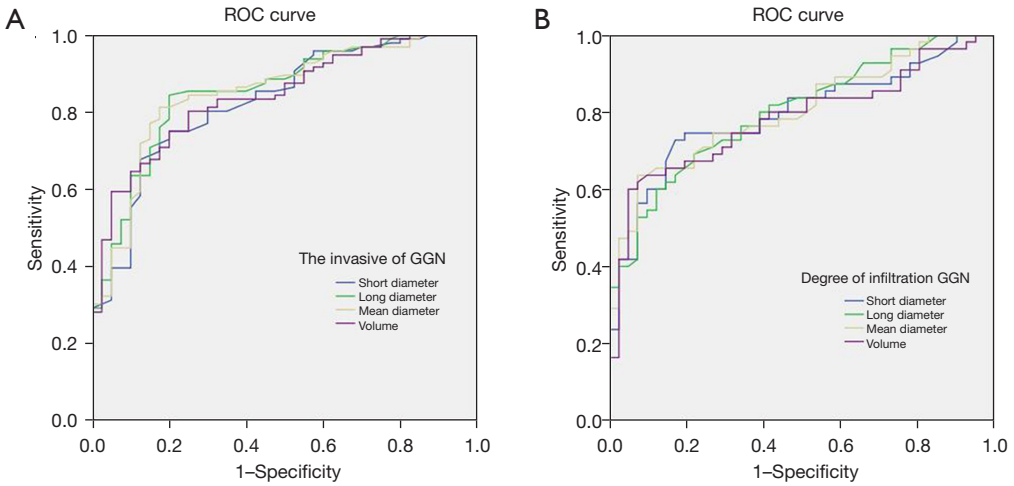

Figure 2 ROC curves of GGN size and volume. (A) Predicting invasion; (B) predicting degree of infiltration. ROC, receiver operating characteristic; GGN, ground-glass nodules.

Table 2 ROC curves showing comparison of sensitivity, specificity, cut-off values, and AUC of nodule diameter line and volumetric on GGN invasion and degree of infiltration

Item	Parameter	Short caliber	Longitudinal	Average diameter	Volume
Invasion	Sensitivity (%)	66.7	84.4	81.3	80.2
	Specificity (%)	87.5	80.0	82.5	75.0
	Cut-off value (HU)	10.40	11.25	10.40	494.12
	AUC	0.827	0.854	0.851	0.841
Degree of infiltration	Sensitivity (%)	72.7	60.0	63.6	60.0
	Specificity (%)	82.9	87.8	92.7	95.1
	Cut-off value (HU)	11.9	17.6	15.73	2,096.44
	AUC	0.794	0.801	0.804	0.782

ROC, receiver operating characteristic; AUC, area under the curve; GGN, ground-glass nodules; HU, Hounsfield unit.

in the binary logistic regression analysis, and the results showed that the nodule morphology (OR =7.087, 95% CI: 1.114–45.101, P=0.038) and bronchial abnormality sign (OR =7.796, 95% CI: 1.562–38.918, P=0.012) were independent risk factors for the degree of GGN infiltration (*Table 5*).

Discussion

The value of general data and qualitative data analysis of GGNs in judging their pathological subtype classification

Recently, the incidence of lung adenocarcinoma has been increasing year by year, accounting for more than 50% of all lung cancers, and it has become the most common type of lung cancer (19). PGLs, MIA and ICA can be manifested as GGNs on thin-section CT. Given the different treatments and regressions of different pathological types of GGN, the identification of invasion and infiltrative degree of GGNs by preoperative CT is of great significance for clinical diagnosis and treatment (20). There was no statistically significant difference in the invasion and degree of infiltration of GGNs in the general data of this study in terms of gender, distribution of lesion location or history of smoking. The difference in age among the three groups was statistically significant, and the invasion and degree of infiltration tended to increase with age; however, logistic

Table 3 Comparison of quantitative parameters among three groups of GGN patients

Groups	Precursor glandular lesion (n=40)	MIA (n=41)	IAC (n=55)	H	P	P1	P2	P3
Plain scan CT attenuation value	−581.17 (−627.66, −526.60)	−551.70 (−580.51, −418.06)	−373.80 (−488.09, −267.54)	43.344	<0.001	0.019	<0.001	0.001
Arterial-phase CT attenuation value	−558.17 (−609.96, −511.20)	−479.95 (−542.61, −370.73)	−326.07 (−436.21, −201.59)	51.678	<0.001	0.004	<0.001	0.001
Venous-phase CT attenuation value	−547.54 (−608.60, −504.78)	−474.40 (−536.93, −359.91)	−297.36 (−405.76, −182.14)	56.247	<0.001	0.006	<0.001	<0.001
ΔCT A-N	19.14 (10.62, 30.66)	40.79 (26.45, 55.20)	56.10 (40.20, 71.89)	48.479	<0.001	<0.001	<0.001	0.020
ΔCT V-N	22.84 (12.79, 41.88)	47.39 (36.31, 62.05)	73.36 (57.87, 98.89)	65.334	<0.001	0.001	<0.001	<0.001
Intensification index A	0.67 (0.60, 0.73)	0.58 (0.44, 0.64)	0.40 (0.25, 0.53)	49.471	<0.001	0.002	<0.001	0.003
Intensification index V	0.65 (0.58, 0.71)	0.54 (0.42, 0.62)	0.35 (0.23, 0.47)	58.878	<0.001	<0.001	<0.001	0.002

The P value represents the overall statistical analysis results among the three groups; (P1, P2, P3 are pairwise comparisons) P1 represents the statistical analysis of precursor glandular lesions and MIA; P2 represents the statistical analysis of precursor glandular lesions and IAC; P3 represents the statistical analysis of MIA and IAC. GGN, ground-glass nodules; MIA, minimally invasive adenocarcinoma; IAC, invasive adenocarcinoma; CT, computed tomography; ΔCT A-N, CT attenuation value arterial phase − CT attenuation value plain scan; ΔCT V-N, CT attenuation value venous phase − CT attenuation value plain scan.

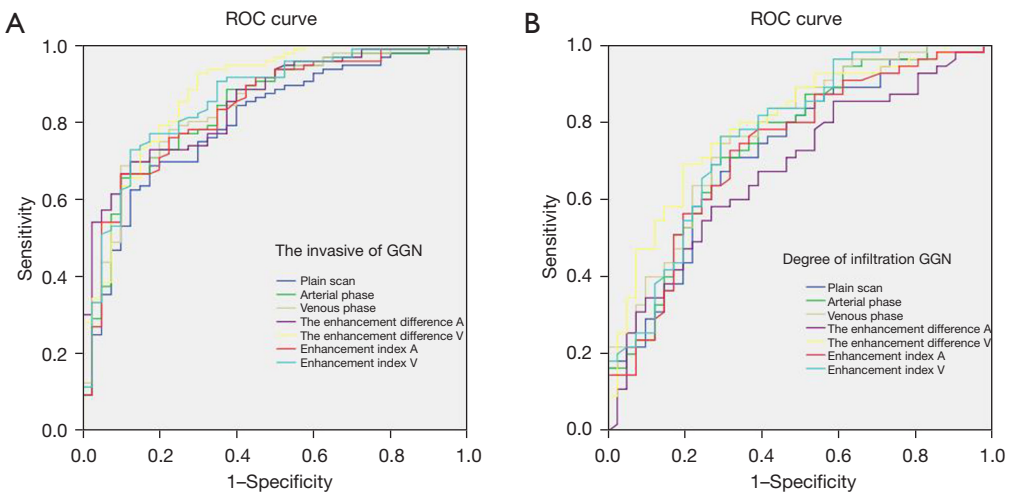

Figure 3 ROC curves of GGN plain scan and enhancement parameters. (A) Predicting invasion; (B) predicting degree of infiltration. ROC, receiver operating characteristic; GGN, ground-glass nodules.

regression analysis showed that age was not an independent risk factor for the invasion and degree of infiltration.

In the univariate analysis of this study, the qualitative data characteristics, such as lesion size, morphology, nodule type, bronchial abnormality sign, internal vascular sign and pleural retraction, showed statistically significant differences among the three groups. The difference between the tumor-lung interface and the vacuole sign was not statistically significant among the three groups. The results of the ROC curve analysis in this study showed that the diameter and volume had high predictive efficacy for GGN invasion, with the long diameter having the best predictive efficacy; a long diameter of 11.25 mm was used as the cut-off value for distinguishing the invasion of GGNs, with a sensitivity of approximately 84% and a specificity of approximately 80%. The predictive efficacy for the degree of GGN infiltration was relatively slightly lower. As the GGN lesions increased in size, their infiltrability tended to increase, which had a

Table 4 ROC curve shows the comparison of sensitivity, specificity, cut-off value, and AUC of CT plain scan and enhanced scan for GGN invasion and infiltration degree

Item	Parameter	Plain scan CT attenuation value	Arterial-phase CT attenuation value	Venous-phase CT attenuation value	ΔCT A-N	ΔCT V-N	Intensification index A	Intensification index V
Invasion	Sensitivity (%)	68.8	65.6	68.8	69.8	92.7	66.7	72.9
	Specificity (%)	82.5	90.0	90.0	87.5	70.0	90.0	87.5
	Cut-off value (HU)	–512.78	–455.98	–452.16	38.28	32.32	0.73	0.70
	AUC	0.800	0.834	0.841	0.850	0.879	0.834	0.856
Infiltration degree	Sensitivity (%)	70.9	69.1	74.5	58.2	69.1	72.7	76.4
	Specificity (%)	68.3	73.2	70.7	73.2	80.5	68.3	76.1
	Cut-off value (HU)	–464.84	–397.87	–401.16	50.45	63.08	0.54	0.51
	AUC	0.729	0.749	0.774	0.780	0.796	0.730	0.770

ROC, receiver operating characteristic; AUC, area under the curve; CT, computed tomography; GGN, ground-glass nodules; HU, Hounsfield unit. ΔCT A-N, CT attenuation value arterial phase – CT attenuation value plain scan; ΔCT V-N, CT attenuation value venous phase – CT attenuation value plain scan.

Table 5 Results of binary Logistic regression analysis of GGN infiltration and degree of infiltration

Item	Variable	B value	Standard error	Wald Chi-square value	P value	OR value	95% CI
Invasion	Nodule type	2.641	0.535	24.371	<0.001	14.026	4.916–40.020
	Vascular abnormality sign	1.848	0.626	8.711	0.003	6.346	1.860–21.646
	Constant	–0.919	0.322	8.131	0.004	0.399	
Degree of infiltration	Nodule morphology	1.958	0.944	4.302	0.038	7.087	1.114–45.101
	Bronchial abnormality sign	2.054	0.820	6.267	0.012	7.796	1.562–38.918
	Constant	–6.454	4.071	2.514	0.113	0.002	

GGN, ground-glass nodules; OR, odds ratio; CI, confidence interval.

certain correlation (21,22), which reported that the size of pGGNs was an independent predictor of invasion; however, the study showed by logistic regression analysis that the size of their GGNs was not an independent predictor of invasion, which may be related to the inclusion of mGGNs in the nodules in this study, which needs to be analysed further.

In this study, according to the overall morphology of GGNs, the round nodules on the CT findings were defined as regular nodules. Regular nodules are more common in PGL and MIA, and irregular nodules are more common in ICA. The mechanism of irregular nodules is mainly related to the inconsistent degree of tumor invasion, unbalanced growth, internal fibrous tissue proliferation and septation. GGNs can be divided into pGGNs and mGGNs according to whether they contain solid components or not. With the appearance of solid components in GGNs, the degree of infiltration showed a gradually increasing trend, which is consistent with the research results of Dong *et al.* (23). With the increase in invasion and degree of invasion of GGNs, the probability of bronchial abnormality signs, internal vascular signs and pleural retraction signs in the lesion increased. The differences between groups were statistically significant, which is similar to the results of previous clinical studies (24,25).

The value of quantitative data analysis of GGN plain scans and enhanced scans in judging the grade of nodular invasion

The main difference between this study and previous studies is that all GGNs in this study underwent enhanced CT scans, and quantitative analysis of plain and enhanced CT scan data showed that there were significant differences

in each CT quantitative index among the three groups. The CT attenuation value in the venous phase had the highest predictive efficiency to distinguish the invasion of GGNs, and its AUC was 0.841. The optimal critical value was –452.16 HU, the sensitivity was 68.8% and the specificity was 90.0%, which further proved the importance of contrast-enhanced scanning in predicting the invasion of GGNs. In addition, in this study, the enhancement difference and intensification index were used to predict the invasiveness of GGNs. The sensitivity and specificity of this study were lower than those of Oh *et al.*, which indicated that CT volumetric density ratios >–300 HU were the best predictors of pGGNs' invasiveness, with a sensitivity of 85% and a specificity of 95% (26). It was found that both methods had good predictive efficacy. In particular, the AUC of the enhancement difference in the venous phase between PGL and invasive lesions was 0.879. To a certain extent, the bias caused by the difference in circulation, scanning time, contrast agent concentration and dosage among patients was avoided. Although the CT attenuation value, enhancement difference and intensification index in each phase were statistically different among the three groups, they were not independent risk factors according to logistic regression analysis; this may be related to the insufficient difference in blood supply between GGN lesions.

Logistic regression was used to analyse the independent risk factors of GGN invasion and invasion degree

The logistic regression analysis in this study suggested that nodule type and vascular abnormality were independent risk factors for the invasion of GGNs. Compared with pGGNs, mGGNs increased the risk of invasion of GGNs. The difference was statistically significant (OR =14.026, 95% CI: 4.916–40.020, P=0.000). The pathogenesis of pGGNs is related to the absence of destruction of alveolar structure, adherent growth of tumor cells and absence of interstitial infiltration. Once invasive tissue occurs, the probability of solid components increases, and CT can show mGGNs. With the increase in the degree of invasion, the density and scope of GGNs gradually increase. Areas with a solid component >5 mm on CT may be related to fibrocyte proliferation and alveolar collapse. In this study, 42 cases of the IAC group had internal vascular signs, and the internal vascular signs were statistically significant for the invasion of GGNs (OR =6.346, 95% CI: 1.860–21.646, P=0.003). It may be that with the increasing degree of malignancy, the demand for blood supply increases and the secretion of stimulating factors increases. This promotes the formation of new blood vessels, the proliferation of surrounding interstitial fibres and fibroblasts, the formation of new blood vessel networks and the tortuosity, stiffness and thickening of blood vessels (27-30). This is consistent with the results of Liu *et al.* (31) who found a significant correlation between vascular abnormalities and nodule infiltration in 316 GGNs.

In the current study, logistic regression analysis revealed that compared to MIA, IAC typically presents with various distinctive features. These include uneven density, irregular shapes, rough edges, lobulation, spiculation, pleural retraction, alterations in the bronchi such as dilatation or stenosis occlusion, and twisted blood vessels. The findings suggest that the morphology of the nodule and signs of bronchial abnormalities are independent risk factors for assessing the extent of infiltration in GGN. Relative to the regular nodules, the irregular nodules increased the risk of developing infiltrative GGN, and the difference was statistically significant (OR =7.087, 95% CI: 1.114–45.101, P=0.038). As the degree of GGN infiltration increased, so did the appearance of nodal irregularities. Bronchial abnormalities status was statistically significant for the occurrence of invasion of GGNs (OR =7.796, 95% CI: 1.562–38.918, P=0.012). With increasing invasion, tumor cells invade surrounding lung tissues and structures, including the bronchi. This may lead to thickening, narrowing or obstruction of the bronchial wall, forming the bronchial anomaly sign. Pre-classifying GGNs radiologically and subsequently comparing these classifications with histological findings could provide a more robust diagnostic tool. This can provide more accurate and targeted guidance for early lung cancer screening plans. For example, clinicians can pay more attention to the evolution and characteristics of pGGNs or mGGNs detected in CT scans, as well as pulmonary nodules with internal vascular signs, to make earlier diagnoses and decide on treatment. This approach may also enable a better understanding of the correlation between imaging characteristics and pathological subtypes of lung adenocarcinoma. Furthermore, as clinicians, we recognise the necessity of establishing reliable parameters to justify observational therapy in patients with GGNs. This study's findings contribute to this need by identifying specific imaging features that correlate with varying degrees of nodule invasiveness. Future studies could further refine these parameters, providing clinicians with more concrete guidelines for managing GGNs, potentially reducing

unnecessary interventions and focusing on patient-centred care. In future research, we can also further investigate the evolution process of PGL and MIA/IAC lesions, as well as possible changes in radiological features, to better understand the reasons for these changes.

There are several limitations in this study. (I) The study involved a limited number of cases and was retrospective without randomisation, introducing potential selection bias. This aspect could significantly contribute to errors, potentially leading to misleading interpretations for the reader. (II) As a single-centre study, our research lacks generalisability and requires validation with data from multiple centres. (III) Since the study lacks longitudinal follow-up, it becomes challenging to evaluate the progression or resolution of the nodules over time, as well as determining the long-term results following resection. (IV) The absence of a comparison group comprising patients with GGNs who have not been subjected to surgical intervention makes it problematic to ascertain the true efficacy of the resection procedures. (V) Manual measurement of the range of CT attenuation value and manual delineation of the ROI of lung tissue cannot avoid all blood vessels, bronchi, etc., and there are no quantitative criteria for the judgment of the solid component within the nodule; all these aspects are subjective and may affect the repeatability of the results. (VI) The lack of data on nodal involvement in patients may influence the study results. (VII) Enhanced CT may increase the radiation dose received by patients and should be fully considered in clinical practice. The application of dual-energy CT in GGNs is a future research direction.

In conclusion, quantitative analysis of CT features combined with enhanced scanning was valuable in predicting the invasion and degree of GGN infiltration, and binary logistic regression analysis suggested that nodule type and signs of vascular abnormality were independent risk factors for predicting the invasion of GGNs. Nodule morphology and bronchial abnormalities were independent risk factors for predicting the degree of GGN infiltration. The radiologic pre-classification of GGNs, compared with the comprehensive analysis of histological results, can provide a more powerful diagnostic tool for physicians and a more effective means for early cancer screening programs, providing more targeted guidance to patients.

Acknowledgments

Funding: This work was supported by the Shandong Province Medical and Health Science Technology Development Plan Project (No. 202209011090).

Footnote

Reporting Checklist: The authors have completed the STROBE reporting checklist. Available at https://qims.amegroups.com/article/view/10.21037/qims-23-1708/rc

Conflicts of Interest: All authors have completed the ICMJE uniform disclosure form (available at https://qims.amegroups.com/article/view/10.21037/qims-23-1708/coif). The authors have no conflicts of interest to declare.

Ethical Statement: The authors are accountable for all aspects of the work in ensuring that questions related to the accuracy or integrity of any part of the work are appropriately investigated and resolved. The study was conducted in accordance with the Declaration of Helsinki (as revised in 2013). The study was approved by inthe ethics committee of Qilu Hospital of Shandong University Dezhou Hospital (Ethics Approval No. 2023009) and individual consent for this retrospective analysis was waived.

References

1. Liu Q, Wang X, Yang Y, Wang C, Zou J, Lin J, Qiu L. Immuno-PET imaging of PD-L1 expression in patient-derived lung cancer xenografts with [68Ga]Ga-NOTA-Nb109. Quant Imaging Med Surg 2022;12:3300-3313.
2. Travis WD, Brambilla E, Noguchi M, Nicholson AG, Geisinger KR, Yatabe Y, et al. International association for the study of lung cancer/american thoracic society/european respiratory society international multidisciplinary classification of lung adenocarcinoma. J Thorac Oncol 2011;6:244-85.
3. Luo YH, Chiu CH, Scott Kuo CH, Chou TY, Yeh YC, Hsu HS, Yen SH, Wu YH, Yang JC, Liao BC, Hsia TC,

Chen YM. Lung Cancer in Republic of China. J Thorac Oncol 2021;16:519-27.
4. Cao M, Li H, Sun D, Chen W. Cancer burden of major cancers in China: A need for sustainable actions. Cancer Commun (Lond) 2020;40:205-10.
5. Sun Y, Xiao L, Wang Y, Liu C, Cao L, Zhai W, Wang B, Yu S, Xin J. Diagnostic value of dynamic (18)F-FDG PET/CT imaging in non-small cell lung cancer and FDG hypermetabolic lymph nodes. Quant Imaging Med Surg 2023;13:2556-67.
6. Adams SJ, Stone E, Baldwin DR, Vliegenthart R, Lee P, Fintelmann FJ. Lung cancer screening. Lancet 2023;401:390-408.
7. Li N, Tan F, Chen W, Dai M, Wang F, Shen S, et al. One-off low-dose CT for lung cancer screening in China: a multicentre, population-based, prospective cohort study. Lancet Respir Med 2022;10:378-91.
8. Yang D, Liu Y, Bai C, Wang X, Powell CA. Epidemiology of lung cancer and lung cancer screening programs in China and the United States. Cancer Lett 2020;468:82-7.
9. WHO Classification of Tumours Editorial Board. Thoracic Tumours (5th ed), International Agency for Research on Cancer, Lyon, France, 2021.
10. Chai W, Jia S, Chen W, Mao D. Character of imaging and follow-up examination in persistent ground-glass opacities on CT scan. J Med Imaging 2017;27:1458-61.
11. Gao L, Zhang J, Gu H, Kang B, Yu X, Zhang S, Gao Y, Cai F, Wang R, Wang X. The value of CT features in predicting the invasion and invasive degree of lung pure ground-glass nodules based on the new classification of lung tumor in 2021. Chin J Radiol 2022;56:616-22.
12. Liu Y, He C, Fang W, Peng L, Shi F, Xia Y, Zhou Q, Zhang R, Li C. Prediction of Ki-67 expression in gastrointestinal stromal tumors using radiomics of plain and multiphase contrast-enhanced CT. Eur Radiol 2023;33:7609-17.
13. Aggarwal A, Das CJ. Contrast-enhanced ultrasound in evaluation of adrenal lesions with CT/MRI correlation. Br J Radiol 2021;94:20201170.
14. Gao C, Xiang P, Ye J, Pang P, Wang S, Xu M. Can texture features improve the differentiation of infiltrative lung adenocarcinoma appearing as ground glass nodules in contrast-enhanced CT? Eur J Radiol 2019;117:126-31.
15. Cuschieri S. The STROBE guidelines. Saudi J Anaesth 2019;13:S31-4.
16. Luo T, Xu K, Zhang Z, Zhang L, Wu S. Radiomic features from computed tomography to differentiate invasive pulmonary adenocarcinomas from non-invasive pulmonary adenocarcinomas appearing as part-solid ground-glass nodules. Chin J Cancer Res 2019;31:329-38.
17. Ricciardi S, Booton R, Petersen RH, Infante M, Scarci M, Veronesi G, Cardillo G. Managing of screening-detected sub-solid nodules-a European perspective. Transl Lung Cancer Res 2021;10:2368-77.
18. Kou J, Gu X, Kang L. Correlation Analysis of Computed Tomography Features and Pathological Types of Multifocal Ground-Glass Nodular Lung Adenocarcinoma. Comput Math Methods Med 2022;2022:7267036.
19. National Health Commission of the People's Republic of China, He J, Wu YL, Gao SG, Wang J. Guidelines for the Diagnosis and Treatment of Primary Lung Cancer (2022 edition). Chin J Rational Drug Use 2022;19:1-28.
20. Wang M, Li L, Zhang J. The value of CT in predicting the invasion of pulmonary pure ground glass nodule. J Med Imaging 2022;32:1496-501.
21. Cheng L, Dou Y, Huang F, Zhang H, Wang D. Quantitative analysis of invasive pulmonary adenocarcinoma as pure ground nodule using MSCT thin-slice reconstruction. J Med Imaging 2022;32:38-41.
22. Heidinger BH, Anderson KR, Nemec U, Costa DB, Gangadharan SP, VanderLaan PA, Bankier AA. Lung Adenocarcinoma Manifesting as Pure Ground-Glass Nodules: Correlating CT Size, Volume, Density, and Roundness with Histopathologic Invasion and Size. J Thorac Oncol 2017;12:1288-98.
23. Dong H, Han Z, Yin L, Qiu Y, Wang X, Yang J, Lou C. Prediction of pathological types of lung ground glass nodules using ultra-HRCT targeted scan. Journal of Practical Radiology 2021;37:1065-8.
24. Mei X, Wang R, Yang W, Qian F, Ye X, Zhu L, Chen Q, Han B, Deyer T, Zeng J, Dong X, Gao W, Fang W. Predicting malignancy of pulmonary ground-glass nodules and their invasiveness by random forest. J Thorac Dis 2018;10:458-63.
25. Gao F, Li M, Ge X, Zheng X, Ren Q, Chen Y, Lv F, Hua Y. Multi-detector spiral CT study of the relationships between pulmonary ground-glass nodules and blood vessels. Eur Radiol 2013;23:3271-7.
26. Oh J, Piao Z, Cho HJ, Chong Y, Kim SS, Kim JH, Kang MW. CT-based three-dimensional invasiveness analysis of adenocarcinoma presenting as pure ground-glass nodules. Transl Cancer Res 2023;12:765-73.
27. Hashimoto H, Matsumoto J, Murakami M, Hiyama N, Yamaguchi H, Kusakabe M, Horiuchi H, Morikawa T. Progressively increasing density of the solid center of a ground-glass nodule in a solitary pulmonary capillary

hemangioma: A case report. Pathol Int 2020;70:568-73.
28. Battista G, Sassi C, Zompatori M, Palmarini D, Canini R. Ground-glass opacity: interpretation of high resolution CT findings. Radiol Med 2003;106:425-42; quiz 443-4.
29. Abdel Razek AAK, Elmokadem AH, Soliman M, Mukherji SK. MR Imaging of Vascular Malformations and Tumors of Head and Neck. Magn Reson Imaging Clin N Am 2022;30:199-213.
30. Niu R, Shao X, Shao X, Wang J, Jiang Z, Wang Y. Lung Adenocarcinoma Manifesting as Ground-Glass Opacity Nodules 3 cm or Smaller: Evaluation With Combined High-Resolution CT and PET/CT Modality. AJR Am J Roentgenol 2019;213:W236-45.
31. Liu L, Wu N, Zhou L, Ma P, Li L, Yang L, Liang X. The correlations between vascular and bronchial abnormality on high resolution CT and the invasiveness of lung adenocarcinoma in subsolid nodules. Chin J Radiology 2019;53:987-91.

Cite this article as: Xie B, Wang R, Fu K, Wang Q, Liu Z, Peng W. The value of predicting the invasiveness and degree of infiltration of pulmonary ground-glass nodules based on computed tomography features and enhanced quantitative analysis. Quant Imaging Med Surg 2024;14(9):6767-6779. doi: 10.21037/qims-23-1708

